RAA 2018 Vol. **18** No. **8**, 92(12pp) doi: 10.1088/1674–4527/18/8/92

http://www.raa-journal.org *http://iopscience.iop.org/raa*

***R**esearch in*
***A**stronomy and*
***A**strophysics*

New variable stars from the photographic archive: semi-automated discoveries, attempts at automatic classification and the new field 104 Her

Sergei V. Antipin[1], Ignacio Becker[2], Alexander A. Belinski[1], Darya M. Kolesnikova[3], Karim Pichara[4,2], Nikolay N. Samus[3,1], Kirill V. Sokolovsky[5,1,6], Alla V. Zharova[1] and Alexandra M. Zubareva[3,1]

[1] P.K. Sternberg Astronomical Institute, M.V. Lomonosov Moscow University, 13, University Ave., Moscow 119234, Russia; *serge_ant@inbox.ru*
[2] Pontificia Universidad Católica de Chile, Santiago, Chile
[3] Institute of Astronomy, Russian Academy of Sciences, 48, Pyatnitskaya Str., Moscow 109017, Russia
[4] Institute for Applied Computational Science, Harvard University, Cambridge, MA, USA
[5] IAASARS, National Observatory of Athens, 15236 Penteli, Greece
[6] Astro Space Center of Lebedev Physical Institute, Profsoyuznaya Str. 84/32, Moscow 117997, Russia

Received 2017 November 25; accepted 2018 January 25

Abstract Using 172 plates taken with the 40-cm astrograph of the Sternberg Astronomical Institute (Lomonosov Moscow University) in 1976–1994 and digitized with a resolution of 2400 dpi, we discovered and studied 275 new variable stars. We present the list of our new variables with all necessary information concerning their brightness variations. As in our earlier studies, the new discoveries show a rather large number of high-amplitude Delta Scuti variables, predicting that many stars of this type remain not detected in the whole sky. We also performed automated classification of the newly discovered variable stars based on the Random Forest algorithm. The results of the automated classification were compared to traditional classification and showed that automated classification was possible even with noisy photographic data. However, further improvement of automated techniques is needed, which is especially important when considering the very large numbers of new discoveries expected from all-sky surveys.

Key words: techniques: photometric

1 INTRODUCTION

The 20th century (more accurately, the time interval between the 1880s and 1990s) was the era of astronomical photography on plates and films. The number of analog photographs at observatories around the world is estimated to be about two million. Information on the existing plate stacks is collected in the Wide-field Plate Database (*www.wfpdb.org*), founded by M.K. Tsvetkov (Bulgaria).

Digitizing plate archives permits users, at the observatories where the archives are stored and elsewhere, to use the vast amount of information when applying modern digital reduction techniques for scientific studies that are important for modern astronomy. It also provides safety against events capable of destroying the analog photographs: fires, floods, etc., like the water main break that occurred at Harvard Observatory on 2016 January 16. Harvard plate stacks, the world-largest collection where about 500 000 sky photographs are kept, fortunately survived the terrible accident due to an effective response from emergency teams, but it is impossible to predict what accident will happen next and where. The process of digitizing Harvard stacks started long before the accident and is under way quite successfully (e.g., Grindlay et al. 2009; *http://dasch.rc.fas.harvard.edu/index.php*).

At Moscow Observatory (now the Sternberg Astronomical Institute of Lomonosov Moscow University, SAI), direct photographs of the starry sky were taken regularly in 1895–1995 using different telescopes, with diameters of their objectives from 10 to 70 cm and focal lengths from 64 to 1050 cm, installed at SAI sites in Moscow, Crimea and elsewhere. The founder of the Moscow plate stacks was Prof. S.N. Blazhko (1870–1956). Details about this plate collection can be found in Shugarov et al. (1999). The total number of sky photographs (direct images) in the Moscow stacks is estimated as 60 000, and they were used in different SAI departments for different purposes.

The most important part of the Moscow plate stacks is 22 300 plates taken with the 40-cm astrograph ($f = 160$ cm, $10^\circ \times 10^\circ$ field of view). This wide-field multi-lens astrograph was initially ordered by C. Hoffmeister (1892–1968) for the Sonneberg Observatory (Germany). In 1938–1945, 1658 sky photographs were obtained with the astrograph. In 1945, it was selected as a part of war reparations by B.V. Kukarkin (1909–1977), at that time an officer in the Soviet Army, later one of the founders of the General Catalogue of Variable Stars. In July, 1948 – April, 1951, the telescope was in operation at Simeiz Observatory, Crimea; in June, 1951 – February, 1958, at Kuchino Observatory near Moscow; in May, 1958, it became the first instrument in operation at the newly established Crimean station of the SAI in Nauchny settlement, Crimea (near the new territory of the Crimean Astrophysical Observatory). At this site, more than 20 800 plates were taken. The limiting magnitude in the central parts of the field, for our typical 45-minute exposure time, is $17 - 18\,\mathrm{mag}B$. Unfortunately, distortions in the plate corners are large, deteriorating the limiting magnitude.

The main purpose of star photographs taken with the 40-cm astrograph was studies of variable stars. The program of observations with the astrograph included many fields. Rich fields contain about 300–500 sky photographs. In cases of overlapping fields, a star can sometimes be found on 700 plates or even more.

We describe our work on digitizing the Moscow plate collection in Section 2. Section 3 presents our new variable-star discoveries. Section 4 deals with statistics related to high-amplitude Delta Scuti (HADS) variable stars in our sample. In Section 5, we discuss an attempt at automated classification of the new variable stars found in this field. Our conclusions are summarized in Section 6. Samus & Li (2018) noted that our attempt at automated classification seemed to be sufficiently successful. We agree with their opinion.

2 DIGITIZING MOSCOW PLATES

Scanning of the plates in the Moscow collection was started in 2006 using two CREO EverSmart Supreme scanners, with resolution of about 2500 dpi. Unfortunately, electronic components in these scanners malfunctioned several years later and could not be repaired. In 2013, following advice from M.K. Tsvetkov, we purchased an Epson Expression 11000XL scanner and continued digitizing our collection using a resolution of 2400 dpi. Due to requirements for funding in Russian science, we decided to arrange the work so that scientific results would not be delayed till the scanning of the whole collection was completed. After finishing digitizing a field, we search for variable stars using the scans and study the discovered variables.

When searching for variable stars, determining their periods and plotting light curves, we commonly use the VaST software package developed by Sokolovsky & Lebedev (2018). VaST relies on SExtractor (Bertin & Arnouts 1996) for detecting sources, and measuring their positions (in pixel coordinates) and brightness.

We apply the following procedure to extract light curves from a series of digitized photographic images for a given sky region.

The grayscale TIFF images produced by the scanner are converted to FITS format using a custom-made code (*ftp://scan.sai.msu.ru/pub/software/tiff2fits/*) and the mid-exposure Julian date (extracted from telescope logbooks) is recorded in the FITS header.

Pixel coordinates of a bright star visible in all images are used as the reference point to cut each image into overlapping $1.2^\circ \times 1.2^\circ$ subfields. The subfields are positioned relative to the reference star and cover the same sky area even for plates that have a large offset from the nominal center of the field. We neglect the plate rotation at this stage, as it is known not to exceed 3° for any of the plates digitized so far.

Then, SExtractor (Bertin & Arnouts 1996) is applied to each subfield image to perform source extraction and circular aperture photometry. The VaST code (Sokolovsky & Lebedev 2018) performs cross-matching of the source lists (as the subfield images are not aligned perfectly) and constructs light curves in an instrumental magnitude scale. As the photographic density is a

non-linear function of the number of incoming photons, we use the relation suggested by Bacher et al. (2005) to convert the measured instrumental magnitudes to the absolute scale set by the B magnitudes of USNO-B1.0 (Monet et al. 2003) stars within each subfield.

Astrometry.net (Lang et al. 2010; Hogg et al. 2008) is used to derive a blind plate solution for each subfield, which is needed to extract equatorial coordinates of the detected objects.

New variables discovered in the course of our project are given provisional variable-star names in the specially introduced Moscow Digital Variable (MDV) series. Test experiments that scanned small parts of plates resulted in discovering MDV 1–MDV 38. The list of these stars can be found in Kolesnikova et al. (2010). The first $10^\circ \times 10^\circ$ field of the 40-cm astrograph, which was completely scanned and searched for variable stars by us, was that centered at the star 66 Oph ($18^\mathrm{h}00.3^\mathrm{m}$, $+04^\circ22'$, J2000.0). In this field, we discovered and studied 480 new variable stars, MDV 39–MDV 518 (Kolesnikova et al. 2008, 2010). The 77 new variable stars discovered in the field of SA9 (the center at $03^\mathrm{h}11.5^\mathrm{m}$, $+60^\circ38'$, J2000.0; MDV 519–MDV 595) are discussed in Sokolovsky et al. (2014). In the present paper, we present our new results obtained in the field centered at the star 104 Her ($18^\mathrm{h}11.9^\mathrm{m}$, $+31^\circ24'$, J2000.0). We have discovered and studied 275 new variable stars.

3 NEW VARIABLE STARS

The plate stacks of the SAI contain 172 plates centered at the star 104 Her ($l = 58^\circ$, $b = 22^\circ$; 1976 March 31 – 1994 October 8). This is a moderately high-latitude field, and the star density is not very high. The plates were scanned with the Epson Expression 11000XL scanner, with resolution 2400 dpi, and searched for new variable stars using the VaST software. Identified variable stars were checked in the GCVS and VSX databases for being new. If photographic data, which have comparatively low photometric accuracy, left doubt as to whether a particular star was variable or not, we checked questionable cases using additional sources of photometric information: the ROTSE/NSVS database (Woźniak et al. 2004b), Catalina database (Drake et al. 2009) and ASAS-SN database (Kochanek et al. 2017). Six stars in the final list were confirmed on the basis of specially arranged CCD observations using telescopes of the SAI Crimean laboratory.

Figure 1 illustrates our technique of photographic photometry and search for variable stars. The VaST code checks all stars deviating along the ordinate from the most densely populated cloud for periodicity; additionally, non-periodic, strongly deviating stars (that can be non-period varies) are inspected by eye. Some of the outliers, those not marked with numbers, are mainly blended stars.

Our final list of newly discovered variable stars is presented in Table 1. It contains 275 new variables (MDV 596–MDV 870).

The columns of Table 1 present: the MDV number of the variable; its equatorial coordinates (J2000.0); its variability type; its period (for period varies); its variability range (photographic B magnitudes at maximum and minimum light, also values for the secondary minimum for eclipsing stars); numbers corresponding to remarks listed at the bottom of the table. The light curves of the variables can be found at our web site (*http://www.sai.msu.su/gcvs/digit/digit.html*).

We performed classification of all the new discoveries using the traditional approach employed by the General Catalogue of Variable Stars team that some of the authors belong to. This classification is principally based on the light curve shape but also takes into account all available additional information (period, amplitude, color index, etc.). Judging from our preferred classifications (the third column of Table 1), more than half of all discoveries (150 stars) are eclipsing variables. Among pulsating variables in Table 1, we often meet RR Lyrae variable stars (70 objects), and semiregular (SR) or irregular (LB, L) stars. There are also eight HADS variables, three Cepheids of the second type (CW), and a variable of the RV Tauri (RVA) type. Two variables are probable rotating spotted stars (type BY:). Figure 2 displays sample photographic light curves for several types of variables. We present our CCD light curves for two stars in Figure 3.

It is very interesting that our photographic search for new variable stars made it possible to also detect low-amplitude variable stars. The lowest peak-to-peak amplitude, $0.1\,\mathrm{mag}$, was found for the EW eclipsing star MDV 640, quite reliably confirmed with data from the ASAS-SN survey.

We will address the period distribution of newly discovered eclipsing variable stars elsewhere. Here we only mention that, for EW stars, this distribution is evidently shifted towards shorter periods, as already noted

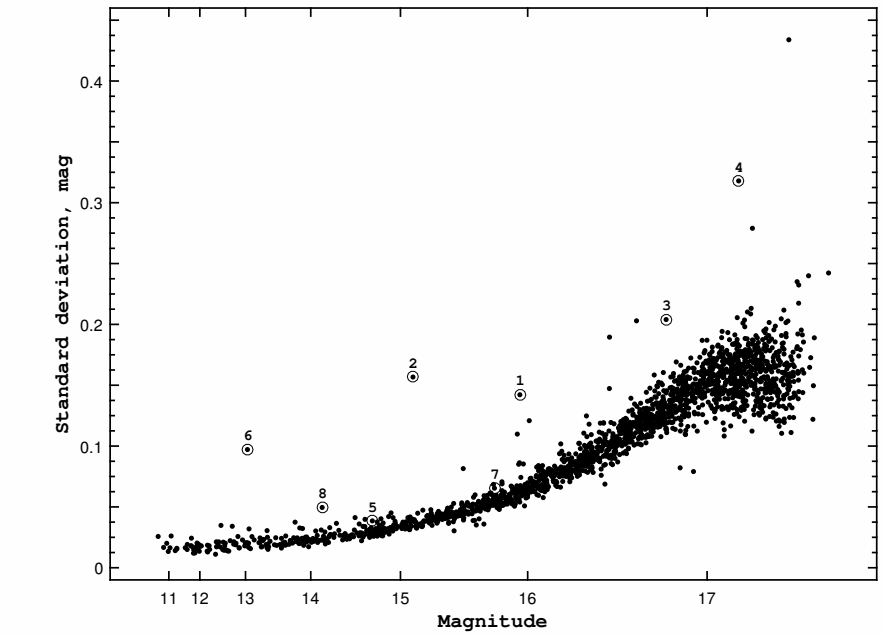

Fig. 1 A diagram illustrating the process of our search for variable stars. The *circled stars* are new or previously known variable stars. 1: NSVS J1812081+302718 (Woźniak et al. 2004a); 2: V1335 Her; 3: MDV 684; 4: MDV 700; 5: MDV 701; 6: MDV 705; 7: MDV 710; 8: MDV 713.

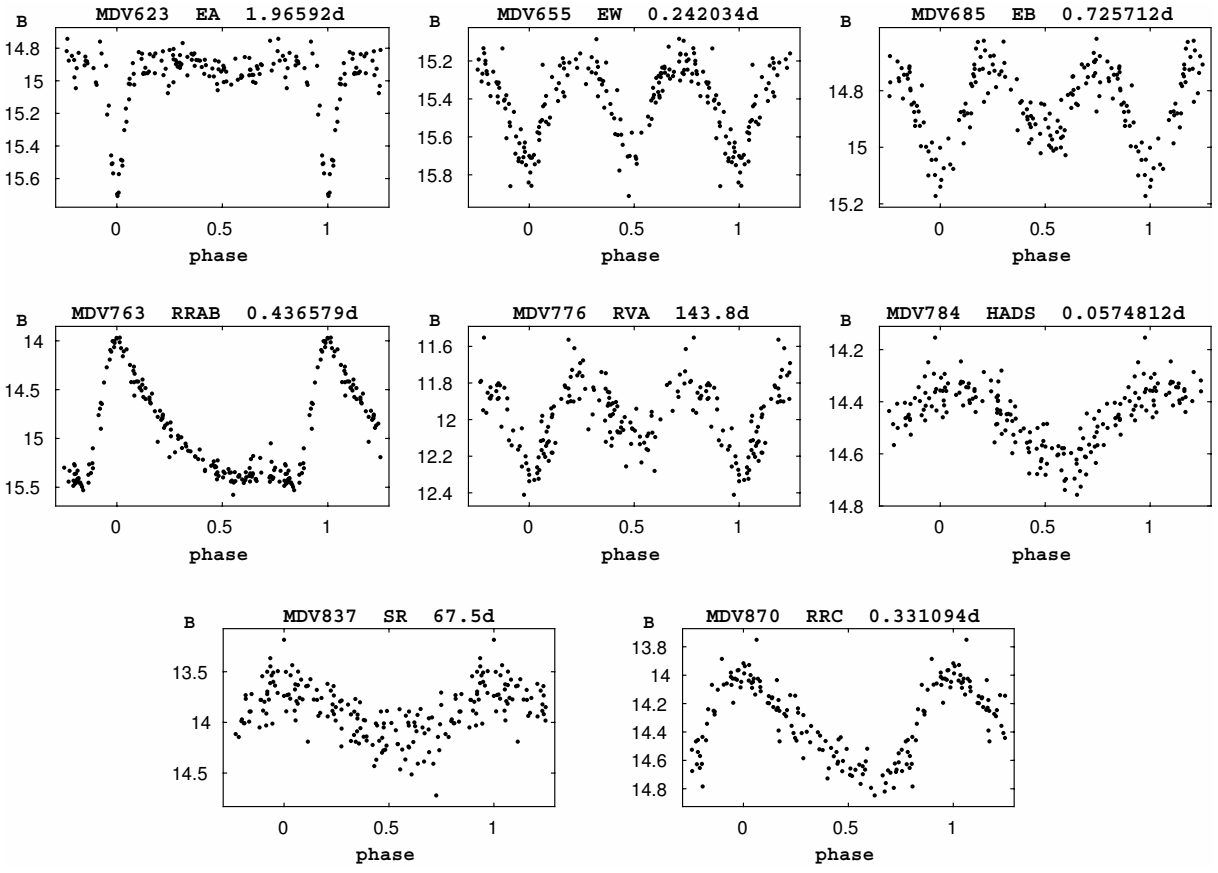

Fig. 2 Sample photographic light curves for some of the new variable stars of different types.

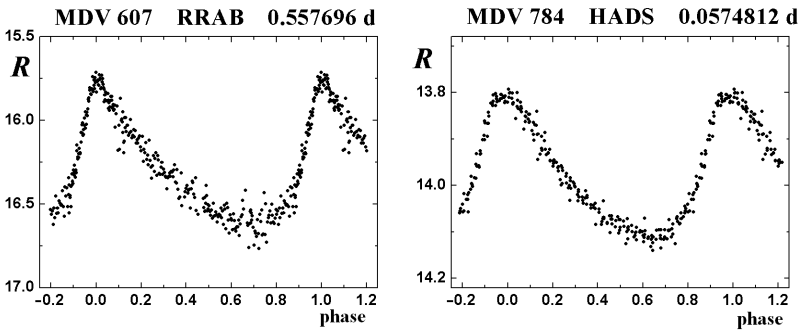

Fig. 3 CCD light curves for two MDV variables.

by Kolesnikova et al. (2010) for our discoveries in the field of 66 Oph.

4 STATISTICS ON HADS VARIABLES

Among short-period pulsating variable stars, a large fraction are Delta Scuti variables, mainly located in the region where the Cepheid instability strip intersects the main sequence. Most of them have small pulsation amplitudes; however, Delta Scuti stars exist with V-band or photographic amplitudes of $0.2\,\mathrm{mag}$ or higher. In most studies, such stars are called HADS variables. This is not a homogeneous variability type but a mixture of younger (Population I) stars and SX Phoenicis variables that belong to old galactic populations. A clear distinction between these variability types has not yet been achieved (see Balona 2016). In the following, we call all large-amplitude, short-period pulsating variable stars HADS variables. Our data do not permit a study of their multiperiodic behavior, which is quite typical for some of them.

From scans of the field centered at 66 Oph, we found 11 HADS stars with peak-to-peak amplitudes of $0.2\,\mathrm{mag}$ or higher. Kolesnikova et al. (2010) remarked that this result lead to the expected number of HADS variables missing from existing variable-star catalogs to be quite large, with the area of the studied field being only 0.24% of the whole area of the sky. The amplitudes of the new HADS variables are not small; they can be easily discovered using photographic plate collections and traditional techniques (eye estimates or measurements with microphotometers).

Expectations for many new HADS variables were not quite fulfilled in the field SA9 (Sokolovsky et al. 2014), where we discovered only one HADS variable.

In the present study, we found eight new HADS variable stars (two of them uncertain); there are also doubts if MDV 790 is an EW or an HADS star, making the total number of new HADS stars nine (three of them are uncertain).

Thus, the total number of HADS discoveries in the field of 300 square degrees (0.73% of the sphere) is from 18 to 21, resulting in an estimate of 2500–3000 for the expected number of HADS stars for the whole sky. This estimate should be additionally somewhat increased because some variables remain undiscovered in the corners of the fields, where the 40-cm astrograph has very large distortions.

As of November, 2017, the electronic version of the 5th edition of the General Catalogue of Variable Stars (GCVS V; Samus et al. 2017) contains 212 stars that can be considered HADS variables (note that the GCVS classification system does not explicitly contain the HADS type, and we had to check classification ourselves). Thus, very many HADS stars remain not included in the GCVS. At first glance, it seems strange; as mentioned above, we are discussing stars with variation amplitudes that are not too low. However, traditional approaches to discoveries of variable stars, their study and their classification could, indeed, fail to find HADS stars because of their short periods. Such periods are no problem for modern computers, but they are not too easy to determine without a computer, as was done in early studies.

5 AUTOMATED CLASSIFICATION OF THE NEW MDV STARS

Several teams are currently developing algorithms that allow automated classification of variable stars from photometric data. Such algorithms are extremely important for future work on variable stars discovered in large-scale projects, like expected discoveries from the *Gaia* space mission. Among the existing algorithms, the majority has

Table 1 New MDV Variable Stars in the Field of 104 Her

MDV	RA, Dec (J2000.0)	Type	Period	Max	Min	Min II	Epoch	Rem
596	17:49:01.69 +31:23:16.2	EB	0.622119	14.30	14.70	14.60	min 2444110.340	[1],[2]
597	17:49:39.63 +33:22:17.0	RRAB	0.572267	16.75	17.80		max 2443671.404	[2]
598	17:50:28.69 +32:30:46.9	SR	54.0	14.60	15.00		max 2443697.3	[1],[3]
599	17:51:05.95 +30:03:06.8	SR	24.5	13.40	13.75		max 2444044.5	[1]
600	17:53:04.73 +28:57:56.4	EW	0.275626	16.20	16.60	16.40	min 2444105.367	[2]
601	17:53:23.23 +29:02:03.8	EB	0.504457	15.75	16.15	15.90	min 2443757.332	[2]
602	17:54:24.12 +28:44:00.8	SR	56.6:	15.10	15.40		max 2443663.4	[2],[4]
603	17:54:36.03 +26:41:33.9	EA	1.775815	15.05	15.50		min 2443786.225	[2]
604	17:54:39.01 +28:27:49.5	L:		11.90	12.50			[5]
605	17:54:49.28 +26:44:32.8	EA	1.22715	15.00	15.35		min 2446357.25	[2]
606	17:55:01.44 +30:36:54.2	EB	0.806310	15.25	15.50	15.45	min 2443757.34	[2]
607	17:55:03.07 +29:19:10.9	RRAB	0.557696	15.90	16.95		max 2443430.232	[6]
608	17:55:33.64 +26:49:51.7	EW	0.277426	15.65	15.95	15.90	min 2443196.416	[2]
609	17:55:52.95 +33:48:12.3	RRC:	0.198706	14.35	14.65		max 2444873.229	[1],[2],[7]
610	17:55:53.33 +28:16:26.4	RRC	0.336777	16.30	16.85		max 2444112.380	[2]
611	17:56:00.95 +28:59:47.3	EA	1.673843	14.80	15.50	15.05	min 2443694.318	[2]
612	17:56:04.66 +33:01:22.9	EA	6.31503	15.25	15.85	15.85	min 2444790.4	[2],[8]
613	17:56:42.28 +31:52:04.4	LB		14.20	14.70			[1]
614	17:56:57.55 +30:21:25.1	EA	0.895829	15.55	16.15	15.75	min 2444456.31	[2]
615	17:57:08.07 +32:54:23.6	LB		11.30	11.80			[1]
616	17:57:09.02 +30:46:03.4	EW	0.282263	15.55	15.80	15.80	min 2445258.225	[2]
617	17:57:09.96 +28:34:17.8	EA	2.76699	13.60	13.90	13.85	min 2442869.50	[2],[9],[10]
618	17:57:36.38 +30:44:07.3	BY:	3.016	16.60	17.10			
619	17:57:43.74 +28:08:09.0	EW	0.372968	16.45	17.00	16.90	min 2444073.419	[2]
620	17:57:46.06 +30:54:39.9	LB		14.90	15.20			[1]
621	17:57:49.15 +31:03:02.6	EW	0.296551	16.70	17.10	17.00	min 2443672.320	[2]
622	17:58:12.27 +26:21:47.4	EW	0.397835	15.95	16.50	16.50	min 2443701.418	[2]
623	17:58:56.10 +31:01:53.0	EA	1.96592	14.85	15.70	14.95	min 2444162.26	[2]
624	17:59:13.03 +27:11:23.6	EW	0.359906	14.25	14.40	14.40	min 2445258.225	[1],[2],[11]
625	17:59:15.09 +30:14:55.5	EW	0.341483	14.95	15.30	15.25	min 2444489.313	[2],[12]
626	17:59:16.44 +33:06:46.5	EW	0.470138	14.60	14.90	14.85	min 2444461.315	[2]
627	17:59:24.01 +27:45:57.0	RRC	0.286315	14.15	14.35		max 2443199.553	[2],[7]
628	17:59:49.75 +29:53:09.1	EW	0.340187	16.05	16.30	16.25	min 2445228.280	[2]
629	18:00:10.98 +32:58:11.2	RRC	0.337218	17.10	17.60		max 2445228.280	[2]
630	18:01:18.15 +27:35:04.7	EW	0.359731	14.70	15.00	14.95	min 2443671.404	[2]
631	18:01:33.73 +34:35:43.6	EA	0.866945	16.10	16.85		min 2444055.447	[2]
632	18:02:07.99 +29:27:52.9	EW	0.401450	14.95	15.20	15.15	min 2443670.382	[2]
633	18:02:11.32 +28:52:06.1	EA	0.727779	16.10	16.80	16.15	min 2443199.553	[2]
634	18:02:34.43 +30:41:22.7	RRAB	0.614662	14.90	15.50		max 2444823.293	[2],[9]
635	18:02:57.31 +27:05:42.5	EW	0.473822	16.10	16.40	16.35	min 2444728.514	[2]
636	18:03:35.03 +32:18:34.9	RRAB	0.646628	15.40	16.90		max 2443691.411	[9],[13]
637	18:03:48.03 +29:15:31.9	EW	0.415536	15.50	15.80	15.75	min 2444107.363	[2]
638	18:04:16.05 +33:37:41.2	RRC	0.378115	15.40	15.90		max 2447676.378	[2],[14]
639	18:04:32.84 +29:39:43.0	RRC	0.333640	14.45	14.60		max 2443787.219	[2]
640	18:04:39.39 +29:47:56.8	EW	0.428358	13.75	13.85	13.85	min 2444463.332	[15]
641	18:04:42.04 +30:41:36.3	EA	0.917043	14.85	15.30	14.95	min 2443695.411	
642	18:04:47.57 +28:14:17.8	RRAB	0.478659	15.80	16.90		max 2443253.482	[2]
643	18:04:49.89 +30:17:20.1	RRC	0.313303	16.45	16.90		max 2445258.225	
644	18:04:51.62 +30:01:29.9	EW	0.383206	15.65	15.90	15.85	min 2444823.293	[2]
645	18:04:55.83 +30:42:00.5	EA	1.84559	13.65	13.85	13.75	min 2444046.39	[1]
646	18:05:09.03 +29:05:24.7	EA	3.0150	13.10	13.40	13.20	min 2443705.47	[1]
647	18:05:12.49 +29:04:40.4	EA	3.4917	15.30	15.60	15.40	min 2444105.37	
648	18:06:11.50 +34:38:51.4	EW	0.523530	14.85	15.05	15.00	min 2444131.333	[2]
649	18:06:17.78 +34:37:48.7	RRAB	0.528967	16.45	17.30		max 2444838.348	[2]
650	18:06:21.99 +32:32:35.5	SR	30.3:	13.75	14.05		max 2443189.6	[16]
651	18:06:22.76 +27:33:24.9	EA	1.75983	15.35	16.00		min 2444876.230	[2]
652	18:06:30.95 +26:59:30.5	EW	0.359248	15.85	16.25	16.15	min 2448778.490	[17]

Table 1 — *Continued.*

MDV	RA, Dec (J2000.0)	Type	Period	Max	Min	Min II	Epoch	Rem
653	18:06:47.02 +28:27:17.1	EW	0.452924	14.15	14.40	14.35	min 2444852.315	[1],[2]
654	18:07:00.47 +27:32:46.5	EB	0.838553	13.95	14.25	14.05	min 2443685.371	[1],[2]
655	18:07:05.27 +30:58:47.8	EW	0.242034	15.20	15.75	15.70	min 2444083.428	[2]
656	18:07:07.52 +32:17:44.0	LB		12.70	13.05			[1]
657	18:07:12.53 +32:54:22.9	CWA:	15.07	15.60	15.90		max 2443705.5	[2]
658	18:07:24.82 +29:29:27.6	EW	0.352261	13.80	14.00	14.00	min 2443691.373	[2]
659	18:07:25.09 +36:02:04.0	EW	0.488014	14.05	14.50	14.35	min 2444818.416	[2]
660	18:07:27.49 +31:29:52.3	EW:	0.485218	16.60	17.30		min 2444875.237	[2]
661	18:07:36.34 +36:00:44.8	EA	1.88865	15.25	15.75		min 2444015.404	[2]
662	18:07:38.46 +30:46:10.6	EW	0.255938	16.20	16.60	16.60	min 2443780.248	[2]
663	18:07:49.22 +32:57:16.4	LB		15.20	16.00			
664	18:07:50.39 +29:17:21.2	EW	0.595814	15.20	15.40	15.40	min 2443694.318	[2]
665	18:08:03.11 +28:53:38.4	RRAB	0.719960	16.40	17.10		max 2444103.301	[2]
666	18:08:36.96 +33:46:27.7	CWA:	16.8	15.25	15.50		max 2443671.4	[18]
667	18:08:56.57 +29:46:51.6	RRAB	0.462302	16.20	17.30		max 2444109.291	[2]
668	18:09:20.36 +33:49:58.1	LB		14.90	15.30			[1]
669	18:09:42.19 +28:18:05.8	RRAB	0.538265	16.20	17.00		max 2443253.482	[2]
670	18:10:23.71 +28:31:08.8	EB	0.491929	14.85	15.10	14.95	min 2444110.340	[2]
671	18:10:36.63 +33:38:53.6	EW	0.388084	14.80	14.95	14.95	min 2445205.333	[1],[12]
672	18:10:37.86 +28:44:03.5	RRAB	0.665442	15.40	16.10		max 2444815.421	[2]
673	18:10:43.76 +28:07:16.5	EW	0.389823	15.10	15.35	15.35	min 2444162.263	[2]
674	18:10:54.53 +32:22:53.2	HADS	0.0847320	16.40	16.75		max 2444876.230	[2]
675	18:11:03.37 +28:07:03.0	EW	0.384549	15.40	15.70	15.60	min 2443282.418	[2]
676	18:11:07.44 +30:47:40.8	EW	0.365738	16.40	16.90	16.80	min 2445258.225	[2]
677	18:11:07.68 +30:51:29.5	EW	0.337050	14.50	14.70	14.60	min 2444053.409	[2]
678	18:11:10.54 +35:38:54.4	RRC	0.322462	16.40	16.75		max 2443282.418	[2]
679	18:11:20.05 +28:53:27.0	RRAB	0.633044	16.15	17.00		max 2444810.340	[2]
680	18:11:31.04 +29:16:10.5	SR	41.9:	13.85	14.05			[19]
681	18:11:32.19 +27:51:32.5	SR	172	14.40	14.70		max 2443670	[20]
682	18:11:33.12 +27:23:03.3	EB	22.9522	15.00	15.80	15.20	min 2444111.4	[2]
683	18:11:52.18 +29:20:24.7	RRC	0.416369	15.25	15.80		max 2444075.403	[2]
684	18:11:53.37 +30:24:50.4	RRAB	0.715046	16.50	17.10		max 2443686.417	[2]
685	18:12:12.49 +29:10:14.7	EB	0.725712	14.70	15.10	14.95	min 2444875.237	[2]
686	18:12:23.90 +33:50:05.7	EB	0.465791	16.05	16.45	16.20	min 2444880.345	[2]
687	18:12:24.30 +28:32:34.6	EA	0.766385	15.60	16.10		min 2444039.356	[2]
688	18:12:29.51 +26:36:01.3	RRAB	0.552409	15.80	16.80		max 2443744.310	[2]
689	18:12:46.79 +27:31:43.9	EW	0.297575	14.90	15.20	15.10	min 2443723.388	
690	18:12:52.34 +29:42:35.5	RRAB	0.549889	15.95	16.55		max 2443253.482	[2]
691	18:12:56.78 +29:13:04.9	RRAB	0.565463	15.50	16.75		max 2443717.377	[2]
692	18:12:58.04 +29:36:25.3	EB	0.387342	15.55	15.80	15.65	min 2443784.222	[2]
693	18:12:58.57 +28:59:28.2	EB	0.741523	15.20	15.35	15.25	min 2444873.229	
694	18:13:18.86 +29:43:31.6	RRAB	0.565299	14.70	15.60		max 2443672.327	[2]
695	18:13:20.08 +31:56:05.8	SR	68.5:	12.80	13.15		max 2444461.3	[21]
696	18:13:33.92 +29:36:44.7	LB		12.10	12.60			[1]
697	18:13:39.28 +28:59:04.8	SR	55.94	15.80	16.50		max 2443744.3	[22]
698	18:14:05.12 +33:50:57.5	EB	0.697571	14.90	15.25	15.00	min 2443722.368	[2]
699	18:14:05.89 +30:49:31.2	RRAB	0.470188	16.80	17.80		max 2443699.457	[2]
700	18:14:15.07 +29:56:13.5	RRAB	0.628599	16.65	17.50		max 2443663.483	[2]
701	18:14:15.68 +30:14:22.2	EW	0.369758	14.65	14.80	14.75	min 2443726.360	[15]
702	18:14:17.99 +27:10:07.6	EA	3.384255	15.50	16.40	15.60	min 2444397.450	
703	18:14:18.07 +27:13:18.1	EW	0.303709	15.60	16.00	15.90	min 2444815.421	
704	18:14:25.46 +27:22:53.6	RRC:	0.281205	16.15	16.60		max 2443934.572	[7]
705	18:14:26.60 +30:11:44.3	LB		11.80	13.40			
706	18:14:31.57 +34:01:47.1	EW	0.326831	13.25	13.45	13.45	min 2444459.318	[9]
707	18:14:38.47 +33:26:42.9	EW	0.323163	14.10	14.30	14.30	min 2443748.313	[2]
708	18:14:43.56 +27:28:39.9	EW	0.309487	14.95	15.20	15.20	min 2446357.247	[23]
709	18:14:43.90 +29:37:52.9	RRC	0.386866	16.05	16.50		max 2442869.499	[24]
710	18:14:44.88 +29:58:29.4	RRC:	0.262310	15.70	15.85		max 2444104.282	[7]

Table 1 — *Continued.*

MDV	RA, Dec (J2000.0)	Type	Period	Max	Min	Min II	Epoch	Rem
711	18:14:46.63 +29:21:05.3	EW	0.272737	15.30	15.65	15.60	min 2444104.282	[2]
712	18:15:02.50 +33:02:29.9	EB	0.665691	15.55	15.80	15.65	min 2444024.407	[2]
713	18:15:13.49 +29:51:56.2	EA	0.885062	14.10	14.75		min 2443717.377	[2]
714	18:15:19.69 +34:24:40.8	EW	0.430040	13.55	13.75	13.75	min 2443934.572	[2]
715	18:15:23.59 +28:14:46.9	EW	0.368195	16.50	17.00	16.85	min 2443759.336	[2]
716	18:15:34.17 +30:16:12.3	EA	0.857063	15.95	16.60	16.40	min 2444075.403	[2]
717	18:15:43.87 +28:17:03.1	EB	0.545438	14.25	14.85	14.40	min 2444085.315	[1],[2]
718	18:15:44.02 +29:16:24.6	EW	0.400190	15.90	16.40	16.20	min 2444821.298	[2]
719	18:15:47.68 +28:25:15.8	EW	0.385311	15.75	16.10	16.05	min 2445228.280	[2]
720	18:16:00.71 +28:28:20.6	RRAB	0.555227	16.40	17.40		max 2443691.411	[2]
721	18:16:02.36 +31:30:13.8	EB:	18.4546	15.40	15.60	15.55	min 2444820.4	
722	18:16:22.12 +27:38:21.8	RRAB	0.504323	15.70	17.10		max 2444838.348	[2]
723	18:16:28.80 +30:00:11.1	RRAB	0.550401	16.30	17.30		max 2444818.416	
724	18:16:37.23 +29:32:33.9	RRAB	0.612923	16.15	16.90		max 2444759.432	
725	18:16:44.90 +32:24:42.7	HADS	0.0761223	16.05	16.30		max 2443671.404	[2]
726	18:16:59.10 +27:25:36.5	EW	0.408681	15.10	15.40	15.30	min 2443701.418	[2]
727	18:17:20.88 +30:04:25.7	EW	0.408577	15.30	15.50	15.45	min 2444456.309	
728	18:17:30.78 +28:55:21.4	RRAB	0.533280	15.40	16.80		max 2444046.393	
729	18:17:38.61 +28:30:23.2	RRC	0.288996	15.85	16.45		max 2443815.196	
730	18:17:40.19 +30:59:23.9	RRAB	0.487686	15.80	17.00		max 2443672.327	[25]
731	18:17:41.94 +30:46:44.9	RRAB	0.555318	15.90	16.90		max 2444458.316	
732	18:18:03.72 +27:03:02.9	HADS	0.115625	15.65	16.05		max 2444110.340	[15]
733	18:18:07.74 +33:26:11.9	LB		14.50	14.75			[1]
734	18:18:08.52 +28:27:35.3	EW	0.358719	16.00	16.35	16.35	min 2444081.379	
735	18:18:12.30 +33:12:58.4	EA	2.14430	14.75	15.35		min 2443754.341	[2]
736	18:18:24.28 +27:55:43.8	EW	0.341269	15.95	16.30	16.30	min 2444823.293	[2]
737	18:18:58.34 +27:11:56.6	EW	0.300959	15.35	15.60	15.55	min 2444781.425	[2]
738	18:19:02.75 +33:46:27.5	SR	51.8	13.30	13.45		max 2444846.4	[26]
739	18:19:07.06 +28:33:07.2	RRC	0.390775	16.65	17.05		max 2444111.411	
740	18:19:13.58 +28:17:35.2	EW	0.303963	14.55	14.70	14.70	min 2444815.421	
741	18:19:17.56 +28:52:44.5	EW	0.375928	14.50	14.90	14.85	min 2444109.291	[1]
742	18:19:19.38 +31:12:16.2	EA	1.51602	15.15	15.70		min 2444397.450	[2]
743	18:19:22.77 +28:29:14.5	SR	29.0	12.40	13.00		max 24437123.4	[27]
744	18:19:23.55 +29:10:58.1	EW	0.332247	15.55	15.80	15.80	min 2444847.395	
745	18:19:30.60 +26:25:51.5	EW	0.318962	15.80	16.30	16.20	min 2443686.327	[1],[2]
746	18:19:32.62 +30:13:38.5	RRAB	0.833771	16.45	17.05		max 2445192.304	
747	18:19:32.83 +29:21:29.2	EW	0.519793	16.60	17.10	17.00	min 2444494.283	[28]
748	18:19:34.10 +30:15:58.0	RRC	0.382189	16.45	17.00		max 2444494.283	
749	18:20:07.41 +32:33:43.0	EB	12.0577	13.75	13.95	13.90	min 2444045.4	[1]
750	18:20:15.45 +33:27:06.2	EW	0.405780	13.35	13.50	13.45	min 2443814.217	[1]
751	18:20:20.06 +34:11:24.5	EW	0.405052	14.10	14.30	14.30	min 2444995.653	[2]
752	18:20:22.49 +34:19:38.5	EA	2.73621	13.35	13.95		min 2444104.282	[1]
753	18:20:23.30 +29:20:39.7	RRAB	0.454574	15.00	16.30		max 2444466.316	
754	18:20:30.58 +29:24:30.0	EB	0.501325	15.05	15.35	15.20	min 2444459.318	
755	18:20:37.05 +30:29:59.3	LB		11.90	12.70			[1]
756	18:20:40.70 +32:16:29.5	SR	47.7	15.35	15.70		max 2443672.3	[29]
757	18:20:50.48 +29:03:24.1	EA	1.08921	15.60	16.15	15.70	min 2443699.457	
758	18:20:56.61 +33:04:52.4	RRAB	0.590969	15.75	16.45		max 2444781.425	
759	18:20:58.93 +28:50:06.6	EW	0.281518	16.30	16.70	16.60	min 2444044.462	
760	18:21:08.37 +29:33:03.8	EW	0.408780	16.55	17.10	16.90	min 2444493.449	
761	18:21:11.26 +32:06:16.0	EW	0.359348	15.95	16.25	16.20	min 2444876.230	
762	18:21:20.39 +31:15:40.5	EW	0.409723	14.45	14.70	14.65	min 2444459.318	
763	18:21:21.91 +30:33:08.7	RRAB	0.436579	13.90	15.45		max 2443783.253	
764	18:21:22.79 +31:06:32.1	EA	1.86917	14.85	15.15	15.00	min 2444459.318	
765	18:21:45.49 +27:39:04.2	EA	2.31034	15.75	16.60	15.85	min 2443757.332	
766	18:21:50.88 +35:51:14.4	SR	204.7	13.60	13.90		max 2449267.2	[29]
767	18:22:02.46 +29:45:42.7	EW	0.388485	14.90	15.15	15.05	min 2444039.356	
768	18:22:11.55 +32:18:50.4	EW	0.377804	15.15	15.40	15.35	min 2444461.315	[9]
769	18:22:12.20 +28:11:59.7	RRC	0.319727	14.55	14.75		max 2444081.379	
770	18:22:27.30 +27:32:34.8	CWA:	13.71	13.95	14.10		max 2444846.36	

Table 1 — *Continued.*

MDV	RA, Dec (J2000.0)	Type	Period	Max	Min	Min II	Epoch	Rem
771	18:22:39.71 +28:30:08.7	EW	0.426878	13.10	13.35	13.30	min 2444112.380	
772	18:22:48.17 +33:17:26.0	EA	1.55636	12.75	12.95	12.85	min 2444847.395	[1]
773	18:23:15.75 +29:16:09.3	EW	0.459035	14.15	14.50	15.45	min 2443697.316	
774	18:23:34.85 +30:50:25.8	SR:	17.94	14.20	14.40		max 2443691.4	[30]
775	18:23:39.28 +29:08:08.5	EW	0.464794	14.90	15.15	15.05	min 2443669.376	
776	18:23:46.16 +28:52:13.6	RVA	143.8	11.75	12.30	12.10	min 2445197.4	[31]
777	18:24:01.70 +28:56:09.6	RRAB	0.564451	14.80	16.20		max 2444106.406	[2]
778	18:24:07.09 +31:29:23.0	EA	0.691002	14.30	14.90	14.35	min 2444044.462	
779	18:24:11.81 +30:57:18.8	SR	56.3:	16.15	16.70			[32]
780	18:24:19.23 +29:54:47.4	EA	0.569231	15.80	16.50	15.90	min 2444109.291	
781	18:24:23.19 +30:39:31.0	RRC	0.290012	15.65	16.25		max 2444077.330	
782	18:24:23.55 +32:57:39.5	EB	0.420047	15.65	16.20	15.85	min 2444877.240	
783	18:24:34.68 +29:22:59.8	RRC	0.330565	13.25	13.45		max 2445197.362	[1]
784	18:24:39.29 +30:32:18.7	HADS	0.0574812	14.35	14.65		max 2443672.327	[6]
785	18:24:40.47 +32:29:00.0	EB	0.475185	16.55	17.10	16.70	min 2445224.286	
786	18:24:41.04 +33:27:28.2	RRAB	0.688098	15.45	16.40		max 2444081.379	
787	18:24:45.24 +30:24:18.4	LB		16.15	16.45			[1]
788	18:24:45.73 +32:12:37.1	LB		14.10	14.80			[1]
789	18:24:54.51 +33:33:18.0	EW	0.438205	15.90	16.30	16.30	min 2443282.418	
790	18:24:57.45 +33:27:05.0	EW:	0.191276	16.40	16.95	16.90	min 2443282.418	[33]
791	18:24:59.85 +30:07:01.3	HADS:	0.0970799	15.20	15.40		max 2444104.282	[15],[7]
792	18:25:07.65 +30:41:13.8	RRC	0.294932	16.50	17.00		max 2444073.419	
793	18:25:16.58 +31:29:39.4	SR	43.5	14.35	14.60		max 2443696.4	[29]
794	18:25:23.86 +26:29:42.7	RRAB	0.754233	15.75	16.25		max 2444015.404	
795	18:25:29.84 +30:23:59.4	RRAB	0.817031	15.80	16.45		max 2444039.356	
796	18:25:35.73 +29:58:26.2	RRAB	0.555571	15.90	17.00		max 2444083.428	
797	18:25:36.04 +29:35:21.4	EW	0.644310	15.65	16.00	16.00	min 2444075.403	[11]
798	18:25:37.36 +33:30:08.2	SR	38.1	12.95	13.15		max 2444141.3	[34]
799	18:25:46.82 +27:40:55.7	RRAB	0.840954	14.40	14.90		max 2443748.313	
800	18:25:59.08 +27:33:10.0	HADS	0.1128665	15.75	16.15		max 2444073.419	
801	18:26:04.44 +35:52:23.6	EW	0.296134	14.40	14.60	14.55	min 2443253.482	
802	18:26:11.38 +33:56:41.9	LB		14.05	14.30			[35]
803	18:26:14.10 +32:18:30.3	EW	0.368156	16.30	16.75	16.65	min 2444875.237	
804	18:26:30.30 +27:40:12.3	RRAB	0.521100	15.55	16.70		max 2443757.332	
805	18:26:33.06 +33:32:41.6	EA	3.48541	13.60	13.85		min 2448401.506	
806	18:26:35.76 +29:52:32.2	RRAB	0.607963	16.30	17.20		max 2447676.378	
807	18:26:55.67 +32:13:25.3	EW	0.419038	14.20	14.65	14.55	min 2444081.379	
808	18:27:04.92 +26:44:34.0	EW	0.399711	15.35	15.85	15.80	min 2444818.416	
809	18:27:10.36 +28:24:08.3	EA	2.00337	15.25	15.80		min 2444077.330	[36]
810	18:27:14.10 +31:26:45.5	EW	0.382948	14.10	14.55	14.50	min 2443803.254	[1]
811	18:27:15.70 +31:00:29.1	EW	0.404429	15.55	15.80	15.75	min 2443813.217	
812	18:27:28.72 +27:35:44.4	EW	0.335950	14.75	15.30	15.30	min 2444277.240	
813	18:27:30.79 +32:57:46.7	EW	0.323209	15.20	15.60	15.50	min 2445230.283	
814	18:27:37.52 +26:52:14.1	EB	0.449438	14.85	15.10	14.95	min 2444073.419	
815	18:27:39.93 +28:14:22.9	RRC	0.298886	16.80	17.20		max 2444106.406	
816	18:27:45.90 +27:54:15.0	RRC	0.289764	15.80	16.30		max 2444104.282	[7]
817	18:27:48.20 +32:13:49.3	LB		13.65	13.90			[37]
818	18:27:49.82 +32:40:20.6	EB	0.460073	15.50	15.85	15.70	min 2444076.345	
819	18:27:54.02 +30:47:19.1	RRC	0.394306	14.60	15.15		max 2443199.553	
820	18:27:56.64 +29:13:05.5	EW	0.401254	15.45	15.90	15.90	min 2444397.450	
821	18:27:57.76 +30:51:34.2	EW	0.321032	16.40	16.80	16.70	min 2443663.483	
822	18:28:15.96 +36:26:25.2	HADS	0.0465770	16.05	16.30		max 2444106.406	[2]
823	18:28:19.92 +26:23:11.5	EA	4.10337	14.00	15.00:		min 2444846.52	[1]
824	18:28:27.20 +28:44:26.1	RRAB	0.590030	16.05	17.05		max 2444821.298	
825	18:28:29.35 +33:45:29.0	EA	1.59798	14.20	14.40	14.25	min 2444790.328	
826	18:28:30.04 +27:38:14.2	EB	0.833553	15.05	15.55	15.50	min 2447328.457	
827	18:28:43.00 +31:39:04.3	EW	0.393631	15.15	15.35	15.35	min 2444164.232	[11]
828	18:28:48.47 +29:41:53.9	EB	0.718740	15.50	16.10	15.80	min 2448401.506	
829	18:29:04.91 +30:52:53.2	RRC	0.345776	13.40	13.55		max 2442869.499	
830	18:29:15.55 +32:34:33.6	E+RS	9.83730	13.30	13.80		min 2443780.248	[15],[38]

Table 1 — *Continued.*

MDV	RA, Dec (J2000.0)	Type	Period	Max	Min	Min II	Epoch	Rem
831	18:29:16.07 +30:50:57.7	LB		13.95	14.30			[39]
832	18:29:20.58 +31:56:48.1	SR	38.5:	14.25	14.55		max 2444839.3	[40]
833	18:29:34.78 +27:07:01.4	LB		14.45	14.75			[41]
834	18:29:39.86 +33:07:04.3	EA	3.14739	15.05	15.65	15.10	min 2444457.310	
835	18:29:41.61 +31:17:57.6	LB		12.85	13.20			[42]
836	18:29:57.15 +29:02:08.3	RRAB	0.607354	16.25	16.70		max 2443776.253	
837	18:30:09.80 +30:43:07.6	SR	67.5	13.60	14.25		max 2444823.3	[43]
838	18:30:20.33 +30:19:23.0	RRC	0.333127	16.20	16.70		max 2444103.301	
839	18:30:22.96 +29:06:43.2	RRAB	0.603389	15.85	16.95		max 2443696.388	
840	18:30:24.56 +31:13:07.6	EW	0.302360	16.15	16.60	16.55	min 2443759.336	
841	18:30:24.59 +29:28:06.9	LB		11.35	11.75			[44]
842	18:30:26.69 +27:21:37.9	SR	44.5:	14.80	15.05		max 2444039.4	[29]
843	18:30:51.02 +32:08:35.6	RRC	0.348948	15.55	16.10		max 2445251.237	
844	18:31:00.79 +30:36:44.4	EW	0.429314	15.90	16.35	16.25	min 2444781.425	
845	18:31:01.58 +33:26:21.8	EW	0.353845	16.15	16.65	16.65	min 2444024.407	
846	18:31:14.97 +27:02:49.3	RRC	0.343227	13.80	14.00		max 2443050.290	[1],[9]
847	18:31:15.83 +34:23:50.4	EA	0.919635	15.75	16.25	15.85	min 2444046.393	[2]
848	18:31:18.42 +26:41:29.5	EW	0.325537	15.10	15.40	15.40	min 2443430.232	
849	18:31:22.62 +30:36:44.8	EB	0.843905	14.80	15.10	15.00	min 2448095.335	
850	18:31:35.22 +27:46:07.5	EB	0.566952	15.30	15.65	15.45	min 2443696.421	
851	18:31:40.81 +32:58:57.9	BY:	7.540	14.15	14.45		max 2443287.4	
852	18:31:48.29 +29:03:21.1	EA	0.952666	14.75	15.20	14.80	min 2443814.217	
853	18:31:57.99 +29:26:04.4	LB		13.65	14.05			[1]
854	18:31:59.77 +29:43:38.5	EA	0.542620	15.75	16.30	15.90	min 2443814.217	
855	18:32:03.89 +32:07:28.3	RRC	0.306341	15.55	16.05		max 2444823.293	
856	18:32:06.20 +26:14:47.8	EB	0.540360	15.05	15.60	15.25	min 2443691.373	[12]
857	18:32:43.73 +28:58:48.3	EW	0.347454	15.20	15.50	15.50	min 2444075.377	
858	18:32:43.98 +29:56:48.3	EW	0.392832	14.60	15.10	15.05	min 2443814.217	[2]
859	18:32:53.51 +30:11:23.3	RRAB	0.592867	14.60	15.55		max 2443814.217	[2]
860	18:33:15.64 +30:58:17.4	LB		13.65	13.90			[15]
861	18:33:17.48 +31:32:57.6	EW	0.330509	13.90	14.20	14.15	min 2443748.313	[1]
862	18:33:31.83 +28:16:18.4	HADS:	0.131393:	16.50	17.10		max 2444025.341	[12]
863	18:33:46.78 +29:50:40.1	EW	0.343149	15.20	15.40	15.40	min 2443718.385	[45]
864	18:33:47.82 +31:47:47.6	CWA:	11.37	16.15	16.45		max 2443699.5	
865	18:34:00.46 +28:59:07.1	EW	0.364373	15.90	16.40	16.35	min 2443672.327	
866	18:34:29.58 +28:41:27.7	RRC:	0.369664	14.85	15.05		max 2444489.313	[7]
867	18:34:51.12 +34:00:20.3	EA	2.72607	16.10	17.05	16.20	min 2443701.418	
868	18:35:04.26 +32:25:13.5	EW	0.375475	15.75	16.05	16.00	min 2443722.368	
869	18:35:26.63 +29:39:14.4	EW	0.502887	15.10	15.90	15.80	min 2443783.253	
870	18:36:56.84 +34:05:57.2	RRC	0.331094	14.00	14.70		max 2443190.574	

Notes: [1] Varies in NSVS data. [2] Varies in Catalina data. [3] From NSVS data, $P = 48.6^{\rm d}$. [4] A small-amplitude variable from NSVS data, $P = 56.6^{\rm d}$ is not detected. [5] A small-amplitude variable from NSVS data, $P = 5.846^{\rm d}$. [6] Our CCD observations confirm variability, type and period. [7] Also possible is type EW with a period twice as long. [8] Min II–Min I = 0.58^P. [9] Double star. [10] A period that is half as short is possible. [11] Also possible is type RRC with a period that is half as short. [12] Our CCD observations confirm variability. [13] The faint component of the pair varies, and photometry from scans merges the two components. The magnitudes in Table 1 are from eye estimates for the faint component. The range from scans for combined brightness is $14.05 - 14.40$ mag. [14] Period varies? [15] Varies in ASAS-SN data. [16] NSVS data suggest $P = 33.1^{\rm d}$. [17] Catalina data suggest $P = 0.359270^{\rm d}$. [18] NSVS data suggest $P = 17.0^{\rm d}$. [19] NSVS data suggest $P = 37.7^{\rm d}$. [20] NSVS data suggest $P = 172^{\rm d}$. [21] NSVS data suggest $P = 77.3^{\rm d}$. [22] NSVS data suggest $P = 54.3^{\rm d}$. [23] $P = 0.236266^{\rm d}$ is also possible. [24] Type EB with a period twice as long is not excluded. [25] Blazhko effect? [26] NSVS data suggest $P = 48.8^{\rm d}$. [27] NSVS data suggest $P = 33.9^{\rm d}$. [28] $P = 0.412568^{\rm d}$ is also possible. [29] Varies in NSVS data, no period. [30] From NSVS data, small amplitude, $P = 17.25^{\rm d}$. [31] NSVS data suggest $P = 143.8^{\rm d}$. [32] NSVS data suggest $P = 53.4^{\rm d}$. [33] Also possible is an HADS type with a period that is half as short. [34] NSVS data suggest $P = 38.3^{\rm d}$. [35] NSVS data suggest type SR and $P = 34.1^{\rm d}$. [36] A period twice as long is possible. [37] NSVS data suggest type SR and $P = 37.1^{\rm d}$. [38] X-ray source 1RXS J182915.3+323440. [39] Emission-line star StHα 151, M0e. [40] NSVS data suggest $P = 43.2^{\rm d}$. [41] ASAS-SN data suggest type SR and $P = 47.4^{\rm d}$. [42] ASAS-SN data suggest type SR and $P = 35.9^{\rm d}$. [43] NSVS data suggest $P = 34.6^{\rm d}$. [44] NSVS data suggest type SR and $P = 49^{\rm d}$. [45] $P = 0.292892^{\rm d}$ is also possible.

been tested only on high-quality photometric data. Our noisy light curves are a real challenge for such programs.

By their nature, light curves are not structured since they are noisy, the number of observations per object depends on the observing strategy and they have missing values. Additional preprocessing must be done by computing statistical descriptors or features. Their mission is to reduce dimensionality and make the data uniform, which can be handled by different algorithms.

Machine learning can be divided into three broad categories: supervised learning, which utilizes labelled data to learn patterns in each class; reinforcement learning, which interacts with the environment such as sensors or a human; and unsupervised learning using just the data to learn patterns, which later can be employed to make visualizations or as inputs for another algorithm.

In their seminal work, Debosscher et al. (2007) constructed a set of 28 features. They were based on analytical fits and periods obtained using the Lomb–Scargle periodogram. They tested this set of features on a Mixture of Gaussians, Neural Networks and Support Vector Machines (SVM, Cortes & Vapnik 1995), obtaining an average precision of 70%. The work of Kim et al. (2011) found that Random Forest (RF, Breiman 2001) outperforms SVM using 11 features. Richards et al. (2011) obtained similar conclusions by including 53 features. Pichara et al. (2012) used a database that included autoregressive features for training an RF, improving previous results. The model was enhanced later by Pichara & Protopapas (2013), who employed graphical models to fill missing data while keeping the computational cost the same.

Since features do not guarantee proper classification, Mackenzie et al. (2016) applied a different approach, developing the first unsupervised feature learning algorithm. It creates a dictionary of words with fragments of the light curves to make a new representation. With them, an SVM classifier was trained, obtaining similar and even better results than the RF while reducing the computational cost significantly.

The initial light curves of the variables in the field of 104 Her were subjected to automated classification based on the RF algorithm since it proved to be the most effective approach.

We implemented the FATS features Python package (Nun et al. 2015) using only time and magnitude fields, as the data do not have uncertainty estimates for each individual measurement. Additionally, they were augmented with 2MASS (Skrutskie et al. 2006) and *WISE* (Wright et al. 2010) colors.

To train the classifier, we used stars earlier announced in the MDV program (Kolesnikova et al. 2010; Sokolovsky et al. 2014). For different reasons, we rejected 18 objects from these lists. In particular, the less represented classes were removed as the RF algorithms cannot generalize a class with a single example. The resulting classes applied for training were: EW (129 stars); LB (115); RRAB (99); EB (62); RRC (60); SR (55); EA (45); HADS (12), for a total of 577 stars.

The result was expressed as a table which listed the three top probabilities of classification, from 0% to 100%, for each variable star. We compared them to the results of our non-automated classification presented in Table 1. The comparison is based on 273 stars; two stars were added to our list of discoveries later.

For 155 stars (57%), the classification in Table 1 coincides with the most probable suggestion from the automated classification. The classification for 85 stars (31%) is that suggested automatically as the second or third option. The non-automated classification disagrees with any option from the automated classification in 12% of all cases.

A frequent case of non-automated classification agreeing with the second or third automated option is that a different type of eclipsing variables is selected. Distinguishing between the EA, EB and EW types is sometimes really somewhat tricky. In our opinion, such cases should also be considered a relative success of the automated technique.

For the stars, the automated classification was least successful (12%). We find that nine stars ($\sim$3%) corresponded to classes that were not represented in the training set, which are usually the most interesting ones. The remaining 24 stars ($\sim$9%) were misclassified even when the class was represented. For noisy light curves of RR Lyrae variables and most of the HADS stars, the classifier tends to decide on the eclipsing types. The SR type was often confused with LB stars. We find that the features cannot distinguish irregularity and semi-regularity as different object classes.

Some interesting cases could not be solved automatically. Thus, the beautiful RV Tauri star MDV 776 received the following type suggestions automatically: SR (probability 56%), LB (probability 43%) and EA (probability 0%). Variable-star astronomers know that variations of RV Tauri stars are indeed semiregular and that

such stars used to show minima that are sharper than maxima.

We hope that further improvement in the algorithm will prevent it from missing stars that are most attractive to astrophysicists. Thus, the automated classification can provide a correct classification for a majority of all stars. Noisy data make the task more difficult (our first attempts used "cleaned" light curves and were more successful). To provide an algorithm completely satisfying to compilers of variable-star catalogs, additional work on the code and its application to noisy data are needed.

One of the possible solutions is to enhance the dataset with OGLE-III V-band variables and gradually retrain the model as new stars are detected and classified.

6 CONCLUSIONS

We continue our work on digitizing photographic plates of the Moscow collection and on finding new variable stars using digitized plates. In this paper, we have presented our results for the $10^\circ \times 10^\circ$ field centered at the star 104 Her.

In total, we discovered 275 new variable stars in the field, mainly eclipsing binaries but also pulsating stars and, possibly, rotating spotted stars. This new study generally confirms our earlier finding that HADS variables are much better represented among the new discoveries than in the General Catalogue of Variable Stars.

The special feature of this study is that we have attempted automated classification of the discovered variable stars based on our photographic photometry. The results were compared to our traditional classification. In 88% of all cases, we were able to achieve good or satisfactory results; the automated classification failed in 12% of cases.

Acknowledgements The authors would like to thank the referee for very valuable suggestions that helped us to improve the manuscript.

References

Bacher, A., Kimeswenger, S., & Teutsch, P. 2005, MNRAS, 362, 542
Balona, L. A. 2016, MNRAS, 459, 1097
Bertin, E., & Arnouts, S. 1996, A&AS, 117, 393
Breiman, L. 2001, Machine Learning, 45, 5
Cortes, C., & Vapnik, V. 1995, Machine Learning, 20, 273
Debosscher, J., Sarro, L. M., Aerts, C., et al. 2007, A&A, 475, 1159
Drake, A. J., Djorgovski, S. G., Mahabal, A., et al. 2009, ApJ, 696, 870
Grindlay, J., Tang, S., Simcoe, R., et al. 2009, in Astronomical Society of the Pacific Conference Series, 410, Preserving Astronomy's Photographic Legacy: Current State and the Future of North American Astronomical Plates, eds. W. Osborn, & L. Robbins, 101
Hogg, D. W., Blanton, M., Lang, D., Mierle, K., & Roweis, S. 2008, in Astronomical Society of the Pacific Conference Series, 394, Astronomical Data Analysis Software and Systems XVII, ed. R. W. Argyle, P. S. Bunclark, & J. R. Lewis, 27
Kim, D.-W., Protopapas, P., Byun, Y.-I., et al. 2011, ApJ, 735, 68
Kochanek, C. S., Shappee, B. J., Stanek, K. Z., et al. 2017, PASP, 129, 104502
Kolesnikova, D. M., Sat, L. A., Sokolovsky, K. V., Antipin, S. V., & Samus, N. N. 2008, Acta Astronomica, 58, 279
Kolesnikova, D. M., Sat, L. A., Sokolovsky, K. V., et al. 2010, Astronomy Reports, 54, 1000
Lang, D., Hogg, D. W., Mierle, K., Blanton, M., & Roweis, S. 2010, AJ, 139, 1782
Mackenzie, C., Pichara, K., & Protopapas, P. 2016, ApJ, 820, 138
Monet, D. G., Levine, S. E., Canzian, B., et al. 2003, AJ, 125, 984
Nun, I., Protopapas, P., Sim, B., et al. 2015, arXiv:1506.00010
Pichara, K., & Protopapas, P. 2013, ApJ, 777, 83
Pichara, K., Protopapas, P., Kim, D.-W., Marquette, J.-B., & Tisserand, P. 2012, MNRAS, 427, 1284
Richards, J. W., Starr, D. L., Butler, N. R., et al. 2011, ApJ, 733, 10
Samus, N. N., Kazarovets, E. V., Durlevich, O. V., Kireeva, N. N., & Pastukhova, E. N. 2017, Astronomy Reports, 61, 80
Samus, N. N., & Li, Y., RAA (Research in Astronomy and Astrophysics), 2018, 18, 88
Shugarov, S., Antipin, S., Samus, N., & Danilkina, T. 1999, Acta Historica Astronomiae, 6, 81
Skrutskie, M. F., Cutri, R. M., Stiening, R., et al. 2006, AJ, 131, 1163
Sokolovsky, K. V., Antipin, S. V., Zubareva, A. M., et al. 2014, Astronomy Reports, 58, 319
Sokolovsky, K. V., & Lebedev, A. A. 2018, Astronomy and Computing, 22, 28
Woźniak, P. R., Williams, S. J., Vestrand, W. T., & Gupta, V. 2004a, AJ, 128, 2965
Woźniak, P. R., Vestrand, W. T., Akerlof, C. W., et al. 2004b, AJ, 127, 2436
Wright, E. L., Eisenhardt, P. R. M., Mainzer, A. K., et al. 2010, AJ, 140, 1868